

# Viscosity measurement with laser-generated and detected shear waves

R. Daniel Costley,<sup>a)</sup> Vimal V. Shah,<sup>b)</sup> Christopher B. Winstead, and J. P. Singh

*Diagnostic Instrumentation and Analysis Laboratories, Mississippi State University,  
205 Research Boulevard, Starkville, Mississippi 39759-9734*

Krishnan Balasubramaniam

*Department of Aerospace Engineering, Mississippi State University, P.O. Box A, Mississippi State,  
Mississippi 39762*

(Received 27 February 1998; accepted for publication 25 November 1998)

A technique is described in which laser-generated shear waves can be used to measure the viscosity of liquids. The technique involves measuring the shear wave reflection coefficient at a solid–liquid interface. To accommodate this procedure, a wedge was designed to launch laser-generated shear waves into the material at nearly normal incidence to the solid–liquid interface. The reflected laser-generated shear waves are detected at a second interface with a laser interferometer. The angle of incidence at this second interface is at an angle greater than the critical angle. The purpose of this arrangement is to maximize the out-of-plane displacement at this second interface so that detection with the interferometer can be more easily accomplished. Calculations that support the design of the wedge and experiment are outlined and experimental results are presented and discussed. This technique would be most applicable in those situations in which conventional techniques are not suitable, such as those involving high temperature and hostile environments. © 1999 Acoustical Society of America. [S0001-4966(99)03803-5]

PACS numbers: 43.35.Cg, 43.35.Yb, 43.35.Zc [HEB]

## INTRODUCTION

Laser-generated ultrasound has great potential in applications where it is difficult or impractical to use a contact transducer. These applications include those in high temperature and corrosive environments.<sup>1–3</sup> This study deals with developing a technique to measure the viscosity of high temperature, and possibly corrosive liquids, such as molten glasses and metals. However, the work presented here is part of a feasibility study, and the experiments have been conducted at room temperature. Future advances and modifications of the technique will adapt it to more hostile environments.

The technique, as explained in more detail in subsequent sections, involved measuring the amplitude of laser-generated shear waves reflected from a solid–liquid interface. This information was used to determine the reflection coefficient, which can be correlated to the viscosity of the liquid. Very few works have dealt directly with laser-generated shear waves. This is probably because the laser is not an efficient shear wave generator, and because in-plane displacements are more difficult to detect than out-of-plane displacements.

Lasers are typically inefficient generators of ultrasound, especially in the thermoelastic regime. Approximately 6% of the energy of an incident light pulse at 1064 nm is absorbed on a clean aluminum surface, the rest being reflected.<sup>1</sup> Not all of the absorbed energy is converted into ultrasound. Of

the energy that is converted into ultrasound in aluminum, approximately 21% is contained within the shear wave, 77% is contained within the Rayleigh wave, and 2% is contained in the compressional wave.<sup>4</sup>

When a shear wave reflects from a surface at normal incidence, the particle motion is entirely within the plane of the surface. Laser interferometers have been developed which can measure these in-plane displacements so that shear waves can be detected directly.<sup>5</sup> In a separate study, a similar interferometer was used to study laser-generated shear waves.<sup>6</sup> Laser-generated shear waves have also been detected with other transducers. Hutchins and Wilkins<sup>7</sup> used electromagnetic transducers to detect laser-generated shear waves and determine their polarization. In a precursor to the work presented here, laser-generated shear waves were detected with piezoelectric shear wave transducers.<sup>8</sup>

The effect of fluid viscosity on reflected horizontally polarized shear waves has been investigated elsewhere.<sup>9–11</sup> Due to the viscosity of a fluid, shear waves can be transmitted into viscous liquid. However, these waves are highly attenuated and rapidly dampen. The capability of the fluid media to convey these waves diminishes the amplitude of the reflected shear waves propagating back into the solid. Thus, the amplitude of these reflected shear waves depends on the capacity of the liquid to transmit them, or its viscosity. The magnitude of the decrease and its relation with the fluid properties will be discussed in the following section.

As mentioned in a preceding paragraph, an earlier study was conducted in which the viscosity of calibration liquids was correlated to the reflection coefficient of laser-generated shear waves.<sup>8</sup> The shear waves were launched with a pulsed Nd:YAG laser into an aluminum wedge and detected using a

<sup>a)</sup>Present address: Military Technology, Inc., P.O. Box 878, University, MS 38677.

<sup>b)</sup>Present address: Halliburton Energy Services, 2135 Hwy. 6 South, Houston, TX 77077.

piezoelectric transducer. This paper describes the results obtained with a totally noncontact system, generating the shear waves with a pulsed laser, and detecting the reflected shear waves with a laser interferometer.<sup>12,13</sup> As part of this project, a wedge was designed so that the laser-generated shear waves are incident to the solid–liquid interface at nearly normal incidence. This causes the relative particle motion between the solid and liquid to be parallel to one another, which is a shearing type motion. The reflection of shear waves at this angle is therefore the most sensitive to viscosity since viscosity is a resistance to shear.

After the shear waves reflect off the solid–liquid interface, they are incident on the surface of detection at greater than the critical angle. This allows for the largest possible out-of-plane displacement. These displacements can then be detected with the more common Mach–Zehnder or Michelson interferometers. This type of arrangement has been used with both aluminum and graphite wedges.

In the following section, the analysis of shear wave reflection from a solid–liquid interface is outlined. Several results from this analysis are presented. The motion of the surface at a solid–air interface is then considered. Results from these two analyses form the basis for the design of the shear wave wedge, an apparatus used to detect laser-generated shear waves. The experimental configuration is described in the following section. In the final section, experimental results obtained with the shear wave wedge are correlated to the viscosity of various calibration liquids.

## I. REFLECTION OF SV WAVES

The reflection of shear waves from a solid–liquid interface is affected by the viscosity and density of the liquid, as well as by the properties of the solid. Earlier work has exploited horizontally polarized shear waves (*SH* waves).<sup>10,11</sup> These are shear waves whose particle motion is parallel to the solid–liquid interface. When these types of shear waves are incident on an interface, only shear waves are transmitted and reflected.<sup>14</sup> However, laser-generated shear waves are vertically polarized, which means that a component of their particle motion is perpendicular to the interface. The exception to this is when the angle of incidence of the vertically polarized shear wave (*SV* wave) is 0 deg, as measured from the normal to the interface. In this case, the two types of shear waves are indistinguishable for an isotropic solid.

### A. Theory

The solution for the reflection coefficient for *SH* waves from a solid–liquid interface is simpler than that for *SV* waves since just one type of wave is transmitted and reflected. However, the solution involving *SV* waves is straightforward, although it involves allowing for the existence of transmitted and reflected compressional waves (*P* waves). The solution outlined in this section follows the procedures presented in textbooks on wave propagation.<sup>14,15</sup> The geometry used in the solution is depicted graphically in Fig. 1 where  $\rho_1$  and  $\rho_2$  represent the density of the solid and liquid, respectively,  $\zeta$  and  $\eta$  represent the bulk and shear viscosities of the liquid, respectively,  $\lambda$  and  $\mu$  are the Lamé

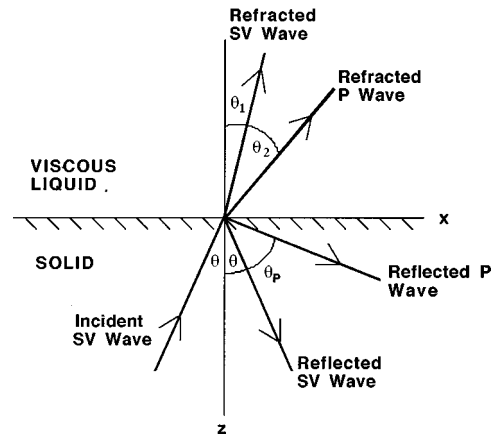


FIG. 1. A graphical representation of a vertically polarized shear wave (*SV* wave) reflecting from a stress-free surface when the angle of incidence is less than the critical angle. The particle motion of the *SV* waves is perpendicular to its direction of propagation, but in the plane of the figure. The particle motion of the compressional wave (*P* wave) is parallel to its direction of propagation.

constants for the solid. In this solution, it is assumed that the displacements are a function of the spatial variables  $x$  and  $z$ , and time,  $t$ . The relevant displacement-boundary conditions are the continuity of the  $x$ - and  $z$ -components of displacement at the interface,  $u$  and  $w$ , respectively. In addition, the normal and shear stresses,  $\sigma_{zz}$  and  $\sigma_{xz}$ , must be continuous across the interface. In the solid, these stresses are written

$$\begin{aligned}\sigma_{zz} &= \lambda \frac{\partial u}{\partial x} + (\lambda + 2\mu) \frac{\partial w}{\partial z}, \\ \sigma_{xz} &= \mu \left( \frac{\partial u}{\partial z} + \frac{\partial w}{\partial x} \right).\end{aligned}\quad (1)$$

If one assumes linear acoustics and harmonic waves of angular frequency  $\omega$  (and using the  $\exp(-i\omega t)$  convention), the stresses in the liquid can be written

$$\begin{aligned}\sigma_{zz} &= (\rho_2 c_0^2 - i\omega\zeta) \frac{\partial u}{\partial x} - 2i\omega\eta \frac{\partial w}{\partial z}, \\ \sigma_{xz} &= -i\omega\eta \left( \frac{\partial u}{\partial z} + \frac{\partial w}{\partial x} \right),\end{aligned}\quad (2)$$

where  $c_0$  is the longitudinal bulk wave speed in the liquid and  $i = \sqrt{-1}$ .

In both the solid and the liquid, the displacements can be expressed in terms of potential functions  $\phi$  and  $\psi$  using the Helmholtz decomposition (for the plane-strain case)<sup>14,15</sup>

$$u = \frac{\partial \phi}{\partial x} - \frac{\partial \Psi}{\partial z}; \quad w = \frac{\partial \phi}{\partial z} + \frac{\partial \Psi}{\partial x}.\quad (3)$$

Displacements in the solid and fluid, and their potentials, are distinguished by the use of the subscripts  $s$  or  $f$ , respectively. In the solid, the potentials can be written

$$\begin{aligned}\phi_s &= P_s e^{ik_p(x \sin \theta_p + z \cos \theta_p)}, \\ \psi_s &= I_s e^{ik(x \sin \theta - z \cos \theta)} + S_s e^{ik(x \sin \theta + z \cos \theta)},\end{aligned}\quad (4)$$

where  $k = \omega/\beta$ ,  $k_p = \omega/\alpha$  and  $\beta$  and  $\alpha$  represent the shear- and compressional-wave speeds in the solid, respectively.

The refracted  $P$  and  $SV$  waves in the viscous liquid are represented by

$$\begin{aligned}\phi_f &= P_f e^{ik_2(x \sin \theta_2 - z \cos \theta_2)}, \\ \psi_f &= S_f e^{ik_1(x \sin \theta_1 - z \cos \theta_1)},\end{aligned}\quad (5)$$

where  $k_2 = \omega/c_0$ ,  $k_1 = \omega/c_1$ ,  $c_1$  is the shear wave speed in the fluid and<sup>16</sup>

$$\begin{pmatrix} -\frac{\beta}{\alpha} \sin \theta_p & \cos \theta & \frac{\beta}{c_1} \cos \theta_1 & \frac{\beta}{c_0} \sin \theta_2 \\ -\frac{\beta}{\alpha} \cos \theta_p & -\sin \theta & \frac{\beta}{c_1} \sin \theta_1 & -\frac{\beta}{c_0} \cos \theta_2 \\ \left(\frac{\beta}{\alpha}\right)^2 \sin 2\theta_p & -\cos 2\theta & -\frac{i\omega\eta}{\mu} \left(\frac{\beta}{c_1}\right)^2 \cos 2\theta_1 & -\frac{i\omega\eta}{\mu} \left(\frac{\beta}{c_0}\right)^2 \sin 2\theta_2 \\ \left(\frac{\beta}{\alpha}\right)^2 \frac{\lambda+2\mu}{\mu} \cos^2 \theta_p & \sin 2\theta & -\frac{i\omega\eta}{\mu} \left(\frac{\beta}{c_1}\right)^2 \sin 2\theta_1 & -\frac{\rho_f c_0^2 - i\omega(\zeta + 2\eta \cos \theta_2)}{\mu} \left(\frac{\beta}{c_0}\right)^2 \end{pmatrix} \begin{pmatrix} \frac{P_s}{I_s} \\ \frac{S_s}{I_s} \\ \frac{S_f}{I_s} \\ \frac{P_f}{I_s} \end{pmatrix} = \begin{pmatrix} \cos \theta \\ \sin \theta \\ \cos 2\theta \\ \sin 2\theta \end{pmatrix}.\quad (7)$$

The displacement in the solid can be represented in terms of the incident  $SV$  wave, reflected  $SV$  wave, and reflected  $P$  wave. In the solid, the  $x$ -component of the displacement turns out to be

$$\begin{aligned}u &= u^I + u^S + u^P, \\ &= ik \cos \theta [I e^{ik(x \sin \theta - z \cos \theta)} - S e^{ik(x \sin \theta + z \cos \theta)}] \\ &\quad + ik_p \sin \theta_p P e^{ik_p(x \sin \theta_p + z \cos \theta_p)}.\end{aligned}\quad (8)$$

The superscripts and coefficients  $I$ ,  $S$ , and  $P$  refer to the incident  $SV$  wave, the reflected  $SV$  wave, and the  $P$  wave, respectively. A similar expression exists for the  $z$  component of the displacement. The total displacement is represented by

$$\begin{aligned}\mathbf{u} &= (u^I + u^S + u^P) \hat{e}_x + (w^I + w^S + w^P) \hat{e}_z, \\ &= \mathbf{u}^I + \mathbf{u}^S + \mathbf{u}^P,\end{aligned}\quad (9)$$

where  $\hat{e}_x$  and  $\hat{e}_z$  are unit vectors in the  $x$  and  $z$  directions, respectively, and  $\mathbf{u}^I = u^I \hat{e}_x + w^I \hat{e}_z$ , etc. The reflection coefficient for  $SV$  waves is defined as

$$R_s = \frac{|\mathbf{u}^S|}{|\mathbf{u}^I|} = \frac{|S_s|}{|I_s|},\quad (10)$$

while the reflection coefficient for  $SV$  waves to  $P$  waves turns out to be

$$R_p \equiv \frac{|\mathbf{u}^P|}{|\mathbf{u}^I|} = \frac{\beta}{\alpha} \frac{|P_s|}{|I_s|}.\quad (11)$$

## B. Solid–viscous liquid interface

It is evident from Eq. (7) that the bulk viscosity,  $\zeta$ , couples with the transmitted  $P$  wave. Due to its nature, the volume viscosity affects mainly the  $P$  wave inside the fluid.<sup>17</sup> Since the second viscosity has little effect on the waves re-

$$c_1^2 = -i\omega \frac{\eta}{\rho_f}.\quad (6)$$

The expressions for the potentials can be substituted into the expressions for the displacements, which can then be substituted into the expressions for the stresses. These equations can be used to represent the boundary conditions at  $z = 0$ . The result of this exercise is four equations which can be written in matrix form:

flected in the solid, it can be neglected. Contrary to the bulk viscosity, the shear viscosity couples with both the incident and reflected  $P$  and  $SV$  waves. Therefore, the reflected  $SV$  wave, as well as the mode-converted  $P$  wave, are sensitive to the shear viscosity of the liquid.

By referring to Eqs. (7)–(11), it can be seen that the reflection coefficient is a function of the angle of incidence and the frequency of the  $SV$  wave, the properties of the solid, and the properties of the liquid. The reflection coefficients for  $SV$  and  $P$  waves as a function of angle of incidence up to the critical angle of the  $SV$  wave are plotted in Fig. 2. For all the examples in this section, the solid is aluminum and the liquid is glycerin unless otherwise noted. At  $0^\circ$ , the reflection coefficient is 0 for the  $P$  wave and nearly 1 for the  $SV$  wave.

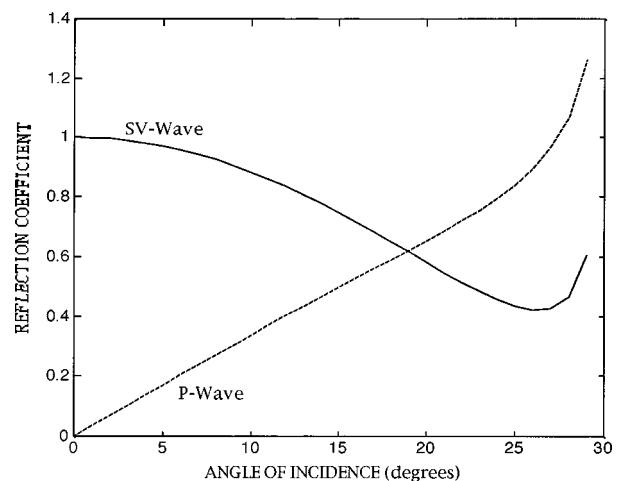


FIG. 2. Reflection coefficient of  $SV$  to  $SV$  and  $P$  waves as a function of angle of incidence at 1.0 MHz. The solid is aluminum, with density 2700 kg/m<sup>3</sup>, shear ( $SV$ ) wave speed 3100 m/s, and compressional ( $P$ ) wave speed 6300 m/s. The liquid is glycerin, with a shear viscosity of 12 poise.

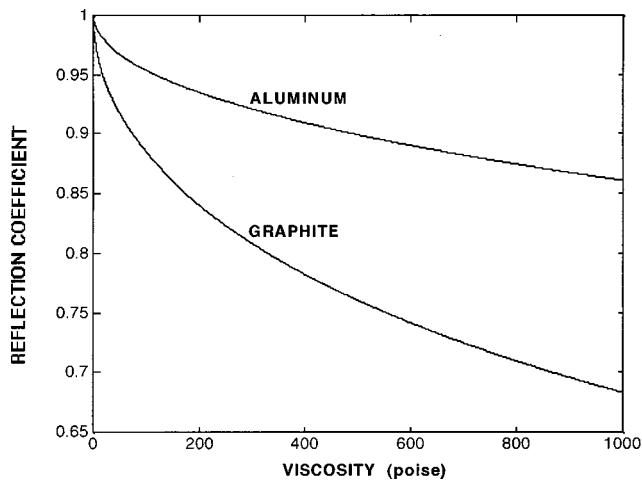


FIG. 3. Reflection coefficient for 1.0 MHz shear waves at normal incidence off a solid–liquid interface for two different solids. The hypothetical liquid has the same density and sound speed as glycerin, which is a 1260 kg/m<sup>3</sup> and 1920 m/s, respectively.

This agrees with the results from the reflection of *SH* waves. The reflection coefficient as a function of the viscosity of the liquid for two different solids is presented in Fig. 3. The curves are for a shear wave at normal incidence, so that no *P* waves are generated. The density and sound speed of the hypothetical liquid were the same as for glycerin: 1260 kg/m<sup>3</sup> and 1920 m/s. As can be seen in the figure, the reflection coefficient for an aluminum–liquid interface is less sensitive to changes in viscosity than for a graphite–liquid interface. This is due to the lower shear wave impedance of graphite. Also, the reflection coefficients for both solids are more sensitive to changes in viscosity at lower viscosities than at higher viscosities, where the magnitude of the slope decreases.

The reflection coefficient for *SV* waves is plotted in Fig. 4 as a function of liquid viscosity for three different angles of incidence (0, 10, and 20°) and two different frequencies (0.5 and 5.0 MHz). For each of the three angles, the higher fre-

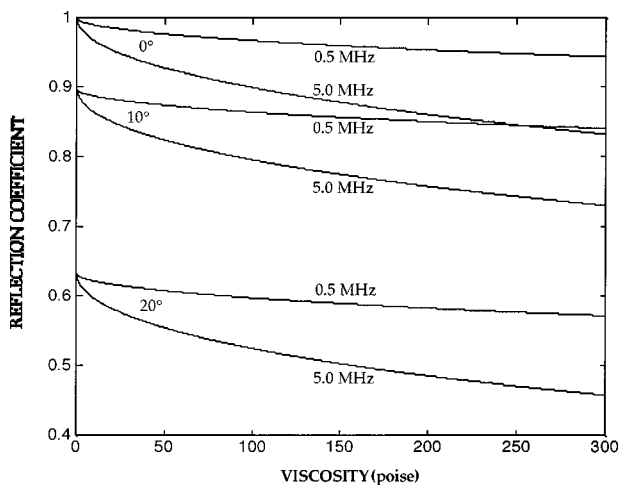


FIG. 4. *SV* wave reflection coefficient,  $R_S$ , as a function of viscosity for different angles of incidence and frequencies. The solid is aluminum and the liquid is a hypothetical liquid with the same density and speed of sound as glycerin, and whose viscosity is varied from 0 to 300 poise.

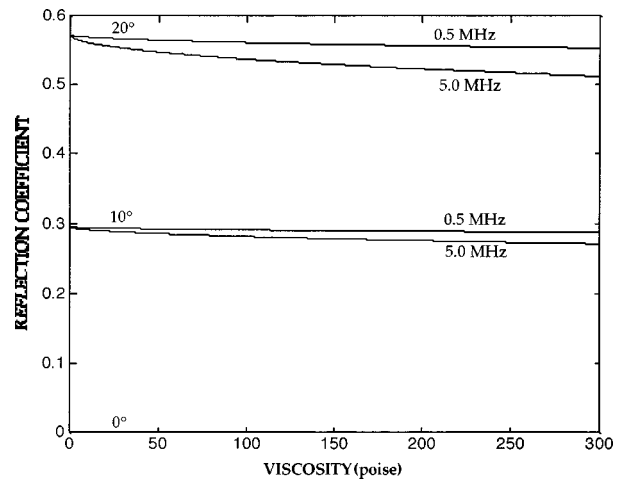


FIG. 5. *SV*-to-*P* wave reflection coefficient,  $R_P$ , as a function of viscosity for different angles of incidence and frequencies. The solid is aluminum and the liquid is a hypothetical liquid with the same density and speed of sound as glycerin, and whose viscosity is varied from 0 to 300 poise.

quency results in a curve with a steeper slope. Thus, the higher frequency would make for a more sensitive determination of viscosity. Also, the figure shows that  $R_S$  decreases as the angle of incidence increases, in agreement with Fig. 2.

The reflection coefficient for *SV* to *P* waves,  $R_P$ , is plotted for two different angles of incidence and two frequencies in Fig. 5. As in Fig. 4, the higher frequency curves have a steeper slope. However, neither curve is very steep, indicating that the reflected compressional wave is not a good indicator of liquid viscosity. In addition, the lower magnitude of this reflection coefficient means that it would be more difficult to detect. Also, note that  $R_P$  increases as the angle of incidence increases, again in agreement with Fig. 2. This is to be expected since, as will be seen in the next section, the interface has more out-of-plane motion at the higher angles of incidence.

In addition to solid and fluid properties, frequency and angle of incidence play significant roles in the magnitude of the reflection coefficients. When designing a system to determine viscosity, it would be desirable that the angle of incidence be at or near normal to the interface. At these angles, the reflection coefficient for *SV* waves is less sensitive to angle. At angles greater than 10° the effect of angle of incidence is more pronounced than the effect of viscosity. In this case, the angle of incidence would have to be determined accurately. In addition, a near-normal angle of incidence will allow for the maximum amplitude of the reflected *SV* wave.

### C. Solid–air interface

When an *SV* wave is incident on a solid–air interface, both an *SV* wave and a longitudinal wave (*P* wave) are reflected when the angle of incidence is less than the critical angle. It is assumed that neither *SV* or *P* waves are transmitted into the air and the solid surface is stress free. The critical angle is defined as the angle of incidence for which the reflected *P* wave propagates parallel to the surface. For an angle larger than the critical angle, which is approximately

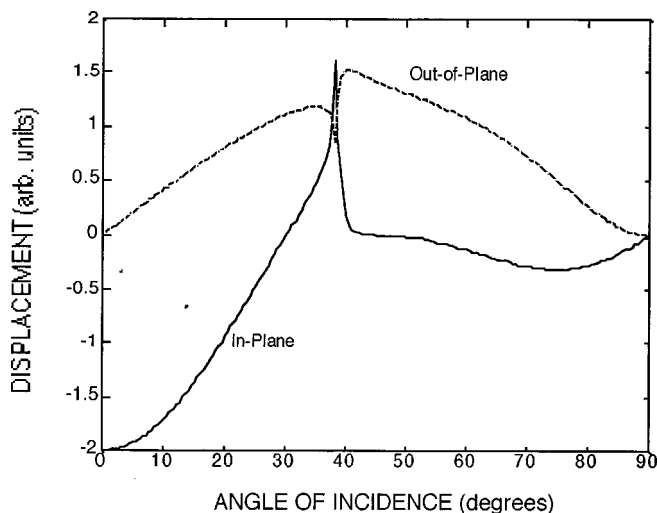


FIG. 6. In-plane and out-of-plane displacements on a stress-free, graphite surface due to an incident *SV* wave. The critical angle is at 38 deg, where the discontinuity occurs.

38° in graphite and 30° in aluminum, the wave number of the *P* wave is complex so that it becomes an evanescent-type wave.

Another consequence of *SV* waves is that, for non-normal incidence, they produce components of displacement that are parallel (in-plane) and normal (out-of-plane) to the surface of the interface. The relative magnitudes of these two components were computed by considering a graphite solid half space, again following procedures presented in several textbooks.<sup>14,15</sup> The surface of the half space was stress free. The situation is similar to that of Fig. 1, except that the viscous liquid is replaced by vacuum, or air. The angle of incidence of the *SV* wave was varied from 0 to 90°. The results of this calculation, which are independent of frequency, were plotted in Fig. 6. As can be seen in the figure, at normal incidence (0°), the total displacement is parallel to the interface (in-plane). The in-plane component starts out negative at 0°, increases to zero, changes sign, and continues to increase up to the critical angle, which in this case is approximately 38°. Both components of displacements have a discontinuity at this point. The out-of-plane displacement increases to a maximum when the angle is just a few degrees greater than the critical angle. In order to detect an *SV* wave incident on a stress-free interface, it would be advantageous for the angle of incidence to coincide with this maximum.

The ultrasound was generated by a pulsed laser on a stress-free surface. Expressions for the directivity patterns of shear waves produced by pulsed-laser sources in the thermoelastic regime have been derived and presented elsewhere.<sup>2,3</sup> They are basically a function of the material properties, specifically Poisson's ratio, and are independent of frequency. Figure 7 shows the directivity pattern for shear waves for a thermoelastic source in aluminum. A distinctive feature of the directivity is the narrow lobe directed at an angle of approximately 30° to the surface normal. We have empirically determined, for several different materials, that the angle at which the maximum occurs corresponds to the critical angle for *SV* wave reflection from a stress-free surface.

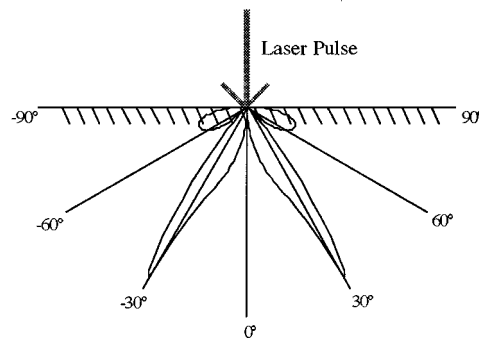


FIG. 7. Directivity pattern for laser-generated shear waves in aluminum.

#### D. Shear wave wedge

The characteristics of laser-generated shear waves discussed in the last section guided the design of a wedge that could be used in the detection of reflected, laser-generated shear waves. These characteristics include their directivity, their reflection from the solid-liquid interface, and their interaction with the solid-air interface. The wedge is depicted in Fig. 8. As shown in the figure, the angle of the wedge is made equal to the critical angle. This causes the narrow lobe of the laser-generated shear wave to be incident at nearly 90° at the solid-liquid interface. The reflection coefficient of an *SV* wave at a solid-viscous liquid interface should be more sensitive to changes in shear viscosity if its angle of incidence is near normal. Intuitively, this seems correct since the shear viscosity is a resistance to a shear type, or in-plane, motion. This angle of incidence also allows for the maximum amplitude of the reflected *SV* wave.

The interferometer beam is located within 5 mm of the spot where the pulsed laser strikes the surface of the wedge. Thus, the angle at which the reflected shear wave is incident at the detector is at a slightly larger angle than the critical angle. As can be seen from Fig. 6, this will produce the largest possible out-of-plane displacement. Thus, it is not necessary, or even advantageous, to use an in-plane detector. These two criteria, normal incidence at the solid-liquid interface and incidence at greater than the critical angle at the solid-air interface where the signal is being detected, were used to design the apparatus used to measure the viscosity of liquids in contact with the appropriate wedge surface.

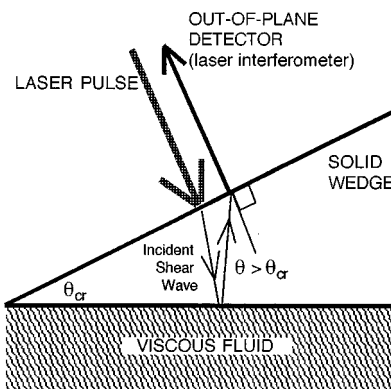


FIG. 8. Schematic of wedge for laser-generated shear wave measurements. The laser pulse and the detection beam are generally separated by less than 5 mm.

## II. EXPERIMENTAL CONFIGURATION

The experimental configuration consisted of an Nd:YAG pulsed laser, a laser interferometer, and a solid wedge as described in the last section. A small plastic container was attached to one side of the wedge to contain the different viscous liquids. The laser beams from the pulsed laser and the interferometer struck the wedge on the opposite side from the viscous liquid, as seen in Fig. 8. A cylindrical lens was used to focus the pulsed-laser beam into a line source. The dimensions of the line source were typically 5 by 1 mm, with some variation between different sets of measurements. The distance between the line source and the interferometer beam was approximately 1–2 mm, again with some variation between sets of measurements. The one-way travel distance of the laser-generated shear waves was approximately 15–20 mm. This was determined by measuring with a ruler from the spot where the lasers hit the wedge along a line that was perpendicular to the viscous-fluid side of the wedge. The distance was also confirmed with time-of-flight measurements.

Because of their close proximity, and to avoid interference problems, it was decided that the pulsed laser and interferometer laser should not be of the same color light. The pulsed laser was an Nd:YAG operating at a wavelength of 1064 nm. The interferometer laser was a frequency-doubled diode-pumped Nd:YAG operating at a wavelength of 532 nm. The interferometer used in this research was a Mach-Zehnder type.<sup>18</sup> It has a bandwidth of approximately 10 MHz and a noise limit of approximately 0.1 nm for a transient pulse. The output of the interferometer electronics is a voltage signal that is proportional to the velocity of the surface at the point of detection.

Voltage waveforms produced by laser-generated shear waves in aluminum and graphite wedges are shown in Fig. 9. The air signal was taken with air in place of the viscous liquid, as shown in Fig. 8. The signals were also averaged to improve the signal-to-noise ratio. All of the signals were averages of at least 100 waveforms.

The shear wave reflection coefficient was calculated as the ratio of the peak-to-peak amplitudes of the viscous-liquid signal to the air signal. Since air has negligible viscosity compared to the viscous liquids, the amplitude of the air signal served to represent the amplitude of the incident signal. In doing this, it was assumed that losses due to geometrical spreading and attenuation in the medium were the same in both the air signal and the viscous-liquid signal. In practice, four air signals and four viscous-liquid signals, as shown in Fig. 9, were acquired, and 16 different reflection coefficients were calculated. These were then averaged, this averaged value was then plotted in Fig. 10. A standard deviation was calculated for each averaged reflection coefficient. The error bars in Fig. 10 represent the average of the s.d.'s calculated for a given experiment. The signals were not converted to units of displacement (e.g., nm) since the voltage signals serve perfectly well for calculating the reflection coefficient ratio.

The work reported in this paper uses broadband ultrasonic signals due to the generation by the laser pulse. The reflection coefficient from a solid–viscous liquid interface is

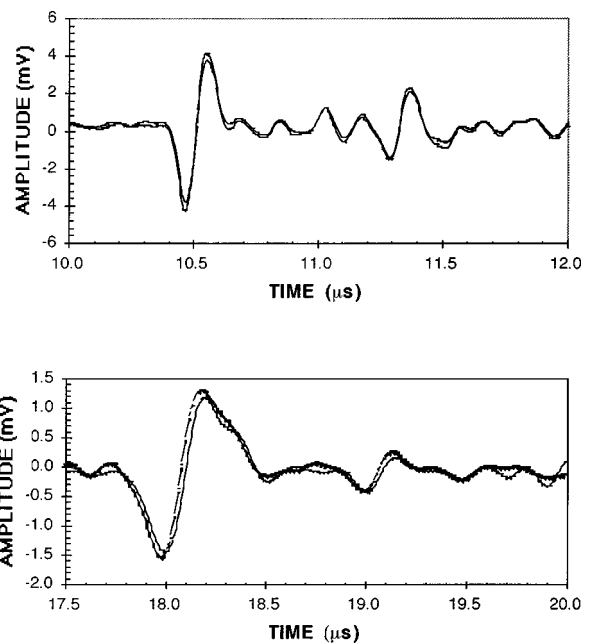


FIG. 9. Reflected, laser-generated shear waves detected in (a) aluminum (at 10.5  $\mu\text{s}$ ) and (b) graphite (at 18.0  $\mu\text{s}$ ) wedges with laser interferometer. In each case, the larger amplitude signal (black line) was the reference acquired with an air-backed wedge. The smaller amplitude signal (gray line) was acquired when the wedge was backed with a viscous liquid.

frequency dependent, as shown in Fig. 4. However, for a given set of measurements, the pulse duration and the size of the laser spot were constant. Thus, the frequency content of the signals was assumed to be similar and the frequency dependence was neglected. A more detailed analysis on this frequency dependence, along with simulations of broadband

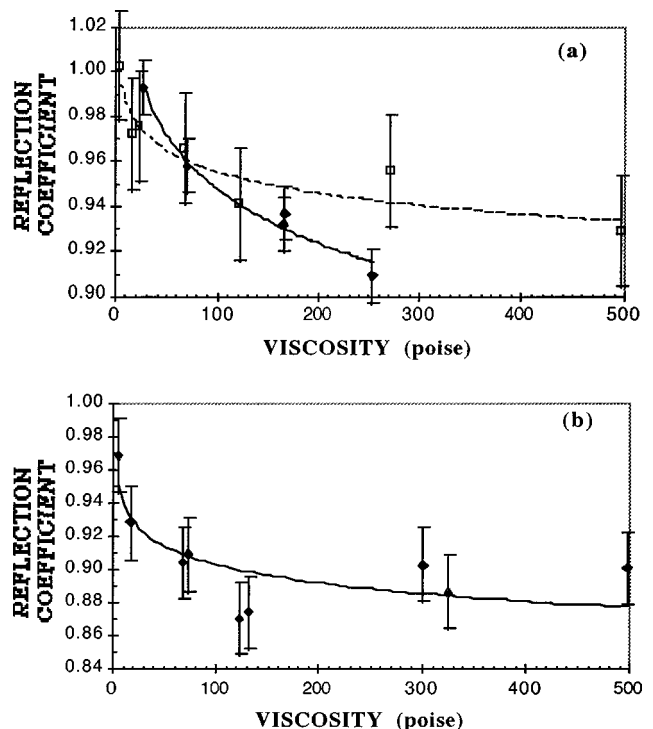


FIG. 10. Viscosity measured with laser-generated SV waves on (a) aluminum and (b) graphite wedges for several different calibration liquids. The solid and dashed lines are second-order polynomial fits to the data.

reflections of shear waves from a solid–liquid interface, has been reported elsewhere.<sup>19</sup>

The differences in laser-pulse energy that generated the air and viscous-liquid signals were neglected in calculating the reflection coefficient. The variations in signal amplitude due to variations in the pulsed-laser energy were minimized by adjusting the *Q*-switch delay of the pulsed laser so that energy output of the laser was at its most stable operating point. Even then, the energy per pulse varied by approximately 10%. Some of this variation was accounted for by signal averaging and the averaging procedure used in calculating the reflection coefficients.

The aluminum and graphite wedges were used to measure the shear wave reflection coefficient from several different viscous liquids. The liquids were certified viscosity standards available through Canon. For each liquid, the viscosity was tabulated at several temperatures. All of the measurements were taken at room temperature, which varied between 20 and 23 °C, and it was assumed that the liquids were at that temperature. The viscosity of the liquid at the recorded room temperature was determined by interpolating along an exponential fit between the tabulated viscosity values. The viscosity of these liquids was plotted against the measured reflection coefficients in Fig. 10. The curves plotted along with the data are trendlines to aid the reader to follow a given set of measurements, and do not represent the theoretical solution.

### III. RESULTS AND DISCUSSION

The plots in Fig. 10 represent the results from three sets of measurements, two with the aluminum wedge and one with the graphite wedge. It can be seen that the data has the same trend as the theoretical curve from Fig. 3, but closer scrutiny shows that the data points do not lie exactly on the theoretical curves.

The two sets of measurements taken on the aluminum wedge are plotted in Fig. 10(a). The waveforms shown in Fig. 9(a) are from the set represented by the solid diamonds in Fig. 10(a). This set of data shows a greater change in the reflection coefficient with viscosity than does the set represented by the open squares. This change in “slope” is probably due to differences in the frequency contents of the signals. It can be seen from Fig. 9 that the signals are broadband, transient pulses. However, the pulse width was slightly different for the two sets. The peak-to-peak distance of the liquid signal in Fig. 9(a) was 86 ns. The peak-to-peak distance of a representative signal from the open square set of data was 113 ns. This represents a lower frequency than the filled-diamond data. The fast-Fourier transforms of the signals support this conclusion. The differences in the frequency content were probably due to small differences in the thickness of the line source. The theoretical results from Fig. 4 show that a lower frequency results in a lower slope.

It can also be seen from Fig. 10(a) that the reflection coefficient of the open squares is less than that of the solid diamonds at the lower viscosities (less than 70 poise). This could be due to differences in the angle of incidence of the *SV* wave at the solid–liquid interface. Figures 2 and 4 show that, for a given frequency and viscosity, the *SV* wave re-

flexion coefficient decreases as the angle of incidence increases (up to 20°). This would mean that the signals corresponding to the open-square data had a larger angle of incidence, as well as a lower frequency.

The results of an experiment conducted with the same viscous liquids and a graphite wedge are plotted in Fig. 10(b). The results show the same trend in the data that was observed with the aluminum wedge; however, there is at least as much scatter. It was suggested in Sec. I.B that the viscosity could be measured with more resolution with a graphite wedge because of its lower shear impedance. However, this seems to be offset by the attenuation of high-frequency ultrasound in the graphite. Since the higher frequencies attenuate significantly more than the lower frequencies, the frequency content of the signal is reduced. This effect lowers the resolution of the viscosity measurements. The frequency dependence of the reflection coefficient for graphite is even more pronounced than that of aluminum, which is shown in Fig. 4.

### IV. SUMMARY AND CONCLUSIONS

A solid wedge was designed to determine the viscosity of liquids using laser-generated shear waves. The shear waves were generated with a pulsed laser and detected with a laser interferometer on the same side of the wedge. The shear waves traveled through the wedge where they reflected from the solid–liquid interface. The reflected wave traveled back to the original side, where it was detected with the laser interferometer. The angle between the two surfaces was such that the reflected shear wave would create the maximum out-of-plane displacement at the detector.

The obvious advantage of such a system is that it is noncontact. This would be especially useful when making measurements at high temperatures. One application of interest is the measurement of glass viscosity in its molten state. Most commercially available piezoelectric transducers used in this application would dipole at these temperatures (1000–1800 °C). In order to use piezoelectric transducers for this application, they would have to be protected from this harsh environment. Mounting it on a water-cooled buffer rod is one solution to this problem.<sup>20</sup> However, in many cases, operators of these facilities do not like this solution because of the possibility of water leaks, which can contaminate the material being processed or create a hazardous situation. Also, cooling may act as a heat sink which cannot be tolerated by many high-temperature processes, as is found in the production of ceramic fibers.<sup>21</sup> The technique described in this paper would eliminate the need for water cooling.

Admittedly, the proposed technique has several disadvantages. These include (a) the need for a special wedge, (b) the relatively high cost of instrumentation, (c) the use of lasers and hence the associated safety issues, and (d) the reduced sensitivity and stability of the interferometric reception of ultrasonic waves when compared with piezoelectric sensors. Another limitation is the lack of resolution, i.e., the reflection coefficient at 5 MHz changes from 1 to 0.84 over a viscosity range of 300 P, as shown in Fig. 4. In spite of these limitations, this method still has the potential to be used in applications where traditional methods cannot be deployed.

These applications include those in hostile environments, inaccessible regions, and, as discussed above, situations where water cooling is not appropriate.

## ACKNOWLEDGMENT

This work was supported by the United States Department of Energy, grant No. DE-FG02-93CH-10575.

- <sup>1</sup>C. B. Scruby, R. J. Dewhurst, D. A. Hutchins, and S. B. Palmer, "Laser Generation of Ultrasound in Metals," in *Research Techniques in Non-destructive Testing*, Vol. 5, edited by R. S. Sharpe (Academic, London, 1982), Chap. 8, pp. 281–327.
- <sup>2</sup>C. B. Scruby and L. E. Drain, *LASER ULTRASONICS: Techniques and Applications* (Hilger, New York, 1990), Chap. 1.
- <sup>3</sup>D. A. Hutchins, "Ultrasonic Generation by Pulsed Lasers," in *Physical Acoustics*, Vol. 18, edited by W. P. Mason and R. N. Thurston (Academic, New York, 1988), pp. 21–23.
- <sup>4</sup>L. R. F. Rose, "Point-Source Representation for Laser-Generated Ultrasound," *J. Acoust. Soc. Am.* **75**, 723–732 (1984).
- <sup>5</sup>J.-P. Monchalain, J.-D. Aussel, R. Heon, C. K. Jen, A. Bouldreault, and R. Bernier, "Measurements of In-Plane and Out-of-Plane Ultrasonic Displacements by Optical Heterodyne Interferometry," *J. Nondestruct. Eval.* **8**(2), 121–133 (1989).
- <sup>6</sup>S. Y. Zhang, M. Paul, S. Fassbender, U. Schleichert, and W. Arnold, "Experimental Study of Laser-Generated Shear Waves Using Interferometry," *Res. Nondestruct. Eval.* **2**(3), 143–156 (1990).
- <sup>7</sup>D. A. Hutchins and D. E. Wilkins, "Polarized Shear Waves Using Laser Line Sources and Electromagnetic Acoustic Transducer Detection," *Appl. Phys. Lett.* **47**(8), 789–791 (1985).
- <sup>8</sup>R. D. Costley, V. Shah, K. Balasubramaniam, and J. P. Singh, "Shear Wave Wedge for Laser Ultrasonics," in *Review of Progress in Quantitative Nondestructive Evaluation*, Vol. 15, edited by D. O. Thompson and D. E. Chimenti (Plenum, New York, 1996), pp. 601–605.
- <sup>9</sup>W. P. Mason, W. O. Baker, H. J. McSkimin, and J. H. Heiss, "Measurement of Shear Elasticity and Viscosities of Liquids at Ultrasonic Frequencies," *Phys. Rev.* **75**(6), 936–946 (1949).
- <sup>10</sup>S. H. Sheen, H. T. Chien, and A. C. Raptis, "An In-Line Ultrasonic Viscometer," in *Review of Progress in Quantitative Nondestructive Evaluation*, Vol. 14, edited by D. O. Thompson and D. E. Chimenti (Plenum, New York, 1995), pp. 1151–1158.
- <sup>11</sup>V. Shah, K. Balasubramaniam, R. D. Costley, and J. P. Singh, "Measurement of Viscosity in Liquids Using Reflection Coefficient ...Phase Difference Method," in *Review of Progress in Quantitative Nondestructive Evaluation*, Vol. 15, edited by D. O. Thompson and D. E. Chimenti (Plenum, New York, 1996), pp. 2067–2071.
- <sup>12</sup>R. D. Costley, C. Winstead, V. Shah, K. Balasubramaniam, and J. P. Singh, "Viscosity Measurement with Laser Ultrasonics," in *Review of Progress in Quantitative Nondestructive Evaluation*, Vol. 16, edited by D. O. Thompson and D. E. Chimenti (Plenum, New York, 1996), pp. 539–545.
- <sup>13</sup>J. P. Singh, K. Balasubramaniam, R. D. Costley, V. V. Shah, and C. Winstead, U.S. Patent 5,686,661 (1997).
- <sup>14</sup>J. D. Achenbach, *Wave Propagation in Elastic Solids* (North-Holland, Amsterdam, 1973), Chaps. 5 and 2.
- <sup>15</sup>A. Bedford and D. S. Drumheller, *Introduction to Elastic Wave Propagation* (Wiley, New York, 1994).
- <sup>16</sup>C. B. Officer, *Introduction to the Theory of Sound Transmission* (McGraw-Hill, New York, 1958), Chap. 6.
- <sup>17</sup>T. A. Litovitz and C. M. Davis, "Structural and Shear Relaxation in Liquids," in *Physical Acoustics*, Vol. 2, edited by W. P. Mason (Academic, New York, 1964), Chap. 5.
- <sup>18</sup>D. A. Bruttomesso, L. J. Jacobs, and R. D. Costley, "Development of an Interferometer for Acoustic Emission Testing," *J. Eng. Mech.* **119**, 2303–2316 (1993).
- <sup>19</sup>V. V. Shah and K. Balasubramaniam, "Effect of Viscosity on Ultrasound Wave Reflection from a Solid/Liquid Interface," *Ultrasonics* **34**, 817–824 (1996).
- <sup>20</sup>V. Shah, K. Balasubramaniam, R. D. Costley, and J. P. Singh, "Sensor Development for High Temperature Viscosity Measurement," in *Review of Progress in Quantitative Nondestructive Evaluation*, Vol. 18, edited by D. O. Thompson and D. E. Chimenti (Plenum, New York, 1998), pp. 853–858.
- <sup>21</sup>J. Righi, U.S. Patent 5,163,620 (1992).